

# Molecular modelling and simulation of electrolyte solutions, biomolecules, and wetting of component surfaces

M. Horsch,<sup>1,\*</sup> S. Becker,<sup>1</sup> J. M. Castillo,<sup>1</sup> S. Deublein,<sup>1</sup> A. Fröscher,<sup>1</sup> S. Reiser,<sup>1</sup> S. Werth,<sup>1</sup> J. Vrabec,<sup>2</sup> and H. Hasse<sup>1</sup>

**Abstract** Massively-parallel molecular dynamics simulation is applied to systems containing electrolytes, vapour-liquid interfaces, and biomolecules in contact with water-oil interfaces. Novel molecular models of alkali halide salts are presented and employed for the simulation of electrolytes in aqueous solution. The enzymatically catalysed hydroxylation of oleic acid is investigated by molecular dynamics simulation taking the internal degrees of freedom of the macromolecules into account. Thereby, Ewald summation methods are used to compute the long range electrostatic interactions. In systems with a phase boundary, the dispersive interaction, which is modelled by the Lennard-Jones potential here, has a more significant long range contribution than in homogeneous systems. This effect is accounted for by implementing the Janeček cutoff correction scheme. On this basis, the HPC infrastructure at the Steinbuch Centre for Computing was accessed and efficiently used, yielding new insights on the molecular systems under consideration.

## 1 Introduction

Molecular simulation provides detailed information on processes on a level which is otherwise inaccessible, on the basis of physically realistic models of the intermolecular interactions. However, despite all efforts to keep these models as simple as possible, such simulations are extremely time consuming and belong to the most demanding applications of high performance computing.

The scientific computing project “*Molecular simulation of static and dynamic properties of electrolyte systems, large molecules and wetting of component surfaces*” (MOCOS) aims at advancing the state of the art by developing the molecular

---

<sup>1</sup>TU Kaiserslautern, Lehrstuhl für Thermodynamik, Erwin-Schrödinger-Str. 44, 67663 Kaiserslautern · <sup>2</sup>Universität Paderborn, Lehrstuhl für Thermodynamik und Energietechnik, Warburger Str. 100, 33098 Paderborn · \*Corresponding author: Martin Horsch, phone: +49 631 205 4028, e-mail: martin.horsch@mv.uni-kl.de

simulation codes *ms2* [1] as well as *ls1 mardyn* [2, 3], and by applying advanced simulation algorithms to complex molecular systems, employing the HPC resources at the Steinbuch Centre for Computing (SCC) in Karlsruhe. Various particular topics of relevance to the project are discussed in detail in dedicated publications to which the interested reader is referred here, concerning modelling and simulation of electrolyte solutions [4, 5], hydrogels [6, 7], and mixtures including hydrogen bonding fluids [8, 9, 10], as well as interfacial phenomena on small length scales [11, 12] and the role of long-range interactions in heterogeneous systems [12, 13].

The present article gives an overview, addressing the three main subjects of the MOCOS project by presenting recent scientific results which were facilitated by the computing resources at SCC: Section 2 discusses molecular model development for ions in aqueous solution and Section 3 reports on molecular simulation of large molecules, i.e. of enzymes and fatty acids. Interfacial phenomena such as the wetting behaviour of fluids in contact with a solid surface are discussed in Section 4 and a conclusion is given in Section 5.

## 2 Molecular modelling of aqueous electrolyte solutions

### 2.1 Force field development for alkali cations and halide anions

Aqueous electrolyte solutions play an important role in many industrial applications and natural processes. The general investigation of electrolyte solutions is, hence, of prime interest. Their simulation on the molecular level is computationally expensive as the electrostatic long range interactions in the solution have to be taken into account by time consuming algorithms, such as Ewald summation [14].

The development of ion force fields in aqueous solutions is a challenging task because of the strong electrostatic interactions between the ions and the surrounding water molecules. Previously published parameterization strategies for the adjustment of the ion force fields of all alkali cations and halide anions yield multiple parameter sets for a single ion [15, 16] or are based on additional assumptions, e.g. the consideration of the aqueous alkali halide solution as a binary mixture of water and cations as well as anions, respectively [17].

The recent study of Deublein *et al.* [18], however, succeeded in obtaining one unique force field set for all alkali and halide ions in aqueous solution. Thereby, the ions are modelled as Lennard-Jones (LJ) spheres with a point charge ( $\pm 1 e$ ) in their centre of mass. Hence, the ion force fields have two adjustable parameters, namely the LJ size parameter  $\sigma$  and the LJ energy parameter  $\epsilon$ . The  $\sigma$  parameter of the ions was adjusted to the reduced liquid solution density. The LJ energy parameter showed only a minor influence on the reduced density and was estimated to be  $\epsilon = 100$  K for all anions and cations [18].

In the present work, the influence of the LJ energy parameter on the self-diffusion coefficient of the alkali cations and the halide anions in aqueous solutions as well as

the position of the first maximum of the radial distribution function (RDF) of water around the ions was investigated systematically. Based on these results, a modified value is proposed for the LJ energy parameter.

The new  $\epsilon_i$  parameter of the ion force fields is determined by a two step parametrization strategy. First, the LJ energy parameter of the ion force fields is adjusted to the self-diffusion coefficient of the ions in aqueous solution. Subsequently, the dependence of the position of the first maximum in the RDF of water around the ions on  $\epsilon_i$  is used to restrict the parameter range derived by considering the self-diffusion coefficient.

## 2.2 Methods and simulation details

In the present study, the self-diffusion coefficient of the ions in aqueous solutions is determined in equilibrium molecular dynamics by the Green-Kubo formalism. In this formalism, the self-diffusion coefficient is related to the time integral of the velocity autocorrelation function [19]. The radial distribution function  $g_{i-O}(r)$  of water around the ion  $i$  is defined by

$$g_{i-O}(r) = \frac{\rho_O(r)}{\rho_{O,\text{bulk}}} \quad (1)$$

where  $\rho_O(r)$  is the local density of water as a function of the distance  $r$  from the ion  $i$  and  $\rho_{O,\text{bulk}}$  is the density of water molecules in the bulk phase. In this case, the position of the water molecules is represented by the position of the oxygen atom. The radial distribution functions are evaluated by molecular dynamics (MD) simulation as well.

The calculation of the self-diffusion coefficient by the Green-Kubo formalism and the evaluation of the RDF is time and memory consuming. The determination of  $D_i$  and  $g_{i-O}(r)$  in electrolyte solutions is considerably more expensive due to additional time consuming algorithms, e.g. Ewald summation [14], required for permitting a truncation of the long range electrostatic interactions; however, it should be noted that a completely explicit evaluation of all pairwise interactions would be even much more expensive.

In a first step, the density of the aqueous alkali halide solution was determined in an isobaric-isothermal ( $NpT$ ) MD simulation at the desired temperature and pressure. The resulting density was used in a canonical ( $NVT$ ) MD simulation at the same temperature, pressure and composition of the different alkali halide solutions. In this run, the self-diffusion coefficient of the ions as well as the radial distribution function, respectively, was determined. In case of the calculation of  $D_i$ , the MD unit cell with periodic boundary conditions contained  $N = 4\,500$  molecules, both for the  $NpT$  and the  $NVT$  simulation run.

For the evaluation of the RDF, there were  $N = 1\,000$  molecules in the simulation volume, i.e. 980 water molecules, 10 alkali cations and 10 halide anions. The radial

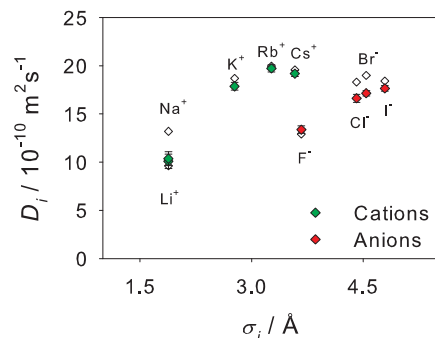


**Fig. 1** Self-diffusion coefficient of alkali cations and halide anions in aqueous solutions ( $x_S = 0.018$  mol/mol) at  $T = 298.15$  K and  $p = 1$  bar. Simulation results (full symbols) are compared to experimental data [20] (empty symbols).

distribution function was sampled in the *NVT* simulation within a cutoff radius of  $15 \text{ \AA}$  with 500 bins.

### 2.3 Self-diffusion coefficients and radial distribution functions

The self-diffusion coefficient  $D_i$  and the position of the first maximum  $r_{\max,1}$  of the RDF  $g_{i-\text{O}}(r)$  of water around the ions was investigated for all alkali cations and halide anions in aqueous solution for  $\epsilon = 200$  K. These data were calculated at high dilution so that correlated motions and ion pairing between the cations and anions were avoided. Hence,  $D_i$  and  $r_{\max,1}$  are independent on the counter-ion in solution.

The results for the self-diffusion coefficient  $D_i$  are shown in Fig. 1. The overall agreement of the simulation results with the experimental data is excellent. The deviations are below 10 % for all ions, except for the sodium cation, where the deviation is about 20 %.

These simulation results also follow the qualitative trends from experiment, i.e.  $D_i$  increases with cation and anion size, respectively. This ion size dependence is directly linked to the electrostatic interaction between the ions and water. In aqueous solution, the cations and anions are surrounded by a shell of electrostatically bonded water molecules (hydration shell). The ions diffuse together with their hydration shell within the bulk water. For small ions, the hydration shell is firmly attached to the ion. Hence, the effective radius, that typically dominates ion motion, is larger for smaller ions than for larger ions, where the hydration shell is less pronounced.

The results of  $r_{\max,1}$  are shown in Fig. 2. In case of the alkali cations, the simulation results are within the range of the experimental data, except for  $\text{Na}^+$  where the deviation from the experimental data is 5.3%. For the halide anions, only the simulation result for  $r_{\max,1}$  of the RDF of water around the iodide anion is within the

range of the experimental data. The deviations of the simulation results for  $r_{\max,1}$  from the experimental data are 12.1 % around  $\text{F}^-$ , 6.5 % around  $\text{Cl}^-$ , and 2.9 % around  $\text{Br}^-$ .

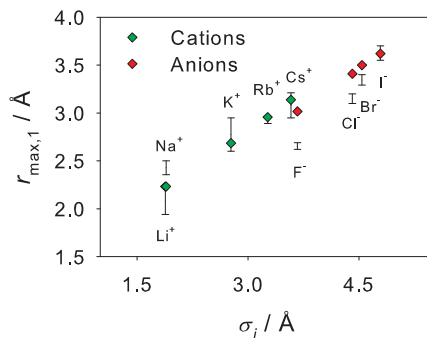


**Fig. 2** Position of the first maximum  $r_{\max,1}$  of the RDF  $g_{i-\text{O}}(r)$  of water around the alkali cations and halide anions in aqueous solutions ( $x_S = 0.01$  mol/mol) at  $T = 293.15$  K and  $p = 1$  bar. Present simulation data (full symbols) are compared to the range of experimental  $r_{\max,1}$  data [21, 22] (vertical lines).

Comparing  $D_i$  and  $r_{\max,1}$  of the cesium cation and the fluoride anion, which have almost the same size, it can be seen that  $\text{Cs}^+$  diffuses faster in aqueous solution and the water molecules of the hydration shell around  $\text{F}^-$  are closer to the ion. This can be attributed to the different orientations of the water molecules around the oppositely charged ions. The water molecules are able to build a stronger attached hydration shell around the fluoride ion which is closer to the ion.

## 2.4 Computational demands

The molecular simulations in Section 2 were carried out with the MPI based molecular simulation program *ms2*, which was developed in our group, cf. Deublein *et al.* [1]. The total computing time for determining the self-diffusion coefficient of ions in aqueous solutions was 138 hours on 36 CPUs (48 hours for the  $NpT$  run and 90 hours for the  $NVT$  run). For these simulations a maximum virtual memory of 1.76 GB was used.

For the evaluation of the radial distribution function of water around the ions a total computing time of 31 hours on 32 CPUs (10 hours for the  $NpT$  run and 21 hours for the  $NVT$  run) was required.

### 3 Simulation of biomolecules with internal degrees of freedom

#### 3.1 Catalysed hydroxylation of unsaturated fatty acids

Producing polymers from regenerative feedstock is a highly interesting alternative to polymers made of naphtha. The first step for obtaining biopolymers is the synthesis and study of all possible basic materials that can be used as building blocks. Such materials can for instance be obtained by an enzymatically catalysed reaction of unsaturated fatty acids to dihydroxy-fatty acids.

In nature, there are only mixtures saturated and unsaturated fatty acids rather than the pure compounds. Therefore, separation – before or after the reaction – is necessary to obtain pure products, e.g. by chromatography, using hydrotalcite as adsorbent and a mixture of water and isopropanol as solvent.

Cytochrome P450 monooxygenase, an enzyme well-known for catalysing the hydroxylation of organic molecules, is a suitable catalyst for this process as well. The critical aspect of the catalytic reaction is the contact between the heme group, which contains the active centre of the enzyme, and the double bonds in the carbon chain of the fatty acid. The enzyme is denaturalized in the presence of organic molecules, and is only active in an aqueous phase. Fatty acids have a small dipole moment and are almost insoluble in water. So how does the contact between the active centre of the enzyme and the fatty acid take place?

A series of molecular simulations was conducted to learn more about the distribution of molecules around the enzyme and the behaviour of the system at different conditions. For this purpose, the mixing behaviour of the systems fatty acid + water, fatty acid + water + isopropanol, and fatty acid + water + cytochrome P450 was investigated. In particular, it is relevant to know whether the fatty acid builds micelles in the water-isopropanol solvent, or how the enzyme catalyses the reaction despite the different phase behaviour of the solvent and the fatty acid. The fatty acid of interest in the present work is oleic acid.

#### 3.2 Simulation details

Molecular simulation of biological systems poses a challenge to scientific computing. The most important limitation in molecular simulation is the system size. As the number of molecules in the simulation box  $N$  increases, the computing time required for the simulation increases with  $O(N^2)$  if it is implemented in a naive way. The reason for this steep dependence is found in the computation of pair potentials, so that the distance and energy between interacting atoms needs to be computed at every simulation step.

One option for decreasing the simulation time consists in following a coarse-graining approach [23]. By coarse-graining, a group of atoms is modelled as a single interaction centre, reducing the number of pair interactions that have to be cal-

culated. As we are interested in obtaining detailed atomistic information, we prefer to use a full atomistic model. The model we selected is OPLS [24], which has been successfully used to simulate a large variety of biological systems. The model for the heme group, inexistent in the original OPLS force field, was taken from a recent parameterization of this group compatible with the OPLS force field [25]. In these models, repulsion-dispersion interactions are treated with LJ potentials, while electrostatic interactions are taken into account considering point partial charges at the atomic positions. Internal molecular degrees of freedom are modelled via bond, bend, and torsion potentials.

The cytochrome P450 enzyme contains more than 7 000 atoms, and together with the fatty acid and the solvent molecules, we need to simulate up to 180 000 atoms. Molecular simulation of such an enormous system would need months of simulation time unless we use advanced parallel simulation programs. For the present simulations of molecular biosystems, the *GROMACS 4.6* MD program was used [26]. At the beginning of the simulation, the molecules were arranged in a randomized fashion within a periodic simulation box, and the energy was minimized. This procedure for generating a starting configuration attempts to mimic experimental conditions where initially the solutions are vigorously mixed. Then every molecule is assigned a random velocity (corresponding to the temperature of the system), and a short simulation of 2 ps is carried out for an initial equilibration. Subsequently, a long simulation (over a minimum simulation time of 20 ns) is run, where the properties of interest are calculated.

The molecular positions are updated using a leapfrog algorithm to integrate Newton's equations of motion. We truncate the LJ potential at a cut-off radius of  $r_c = 1.5$  nm, and use the particle-mesh Ewald summation method [27] to calculate electro-

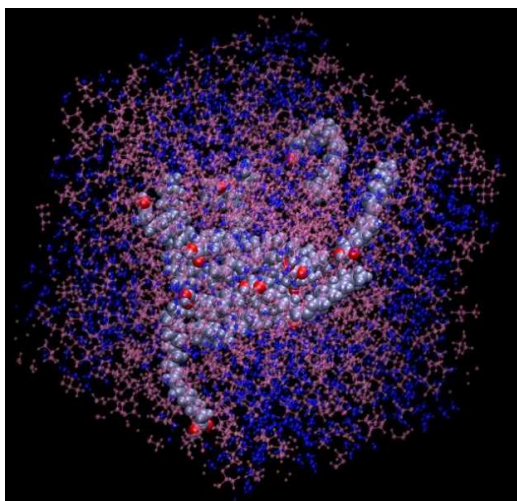


**Fig. 3** Cluster of oleic acid molecules in water-isopropanol solution. Dark blue, water; violet, isopropanol; light blue, oleic acid. The acid group of the oil molecules is painted in red.

static interactions. Temperature is controlled by velocity rescaling with a stochastic term, and pressure with a Berendsen barostat. More details about these simulation techniques can be found elsewhere [28].

Our simulations are performed under conditions for which reliable experimental data are available, i.e. at a temperature of 298 K and a pressure of 100 kPa. For the water-oleic acid system, we use a fatty acid mass fraction of 60 % and two different simulation boxes with approximately the same volume: A cubic box with  $V = (7.14\text{nm})^3$ , and a orthorhombic box of the dimension  $5 \times 15 \times 5 \text{ nm}^3$ . For the isopropanol-water-oleic acid system, we added 10 mg/ml of oleic acid to a mixture water/isopropanol with a mass fraction of 60 % (for isopropanol) in a cubic simulation box of  $(12 \text{ nm})^3$ . Finally, the oil/water concentration in the cytochrome P450 + water + oil system corresponded to a volume fraction of 30 % (for oleic acid) in a cubic box of  $(10 \text{ nm})^3$ , wherein a single cytochrome P450 enzyme was placed.

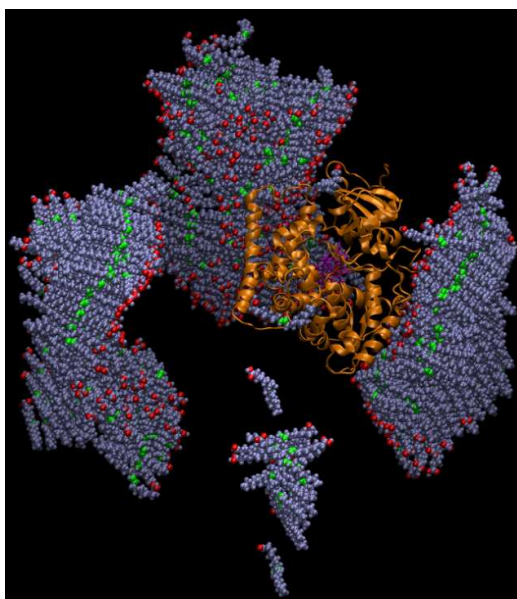


**Fig. 4** Cytochrome P450 in water-oleic acid solution. Cytochrome P450 is painted in orange; the heme group, in violet; the oil molecules, in light blue. The acid group of the oil molecules is painted in red, the double bond in green. For clarity, water has been removed in the picture.

### 3.3 Simulation results

Molecular simulations of oil in the presence of water show a swift phase separation, as it is expected from experimental observation. The phase separation takes place

only after a few picoseconds. Independently of the shape of the simulation box, the oleic acid forms a bilayer, while other possible structures are not observed. Oil molecules form an ordered phase, where their acid groups point in the direction of the water phase, and their hydrocarbon tails are aligned. This is a consequence of the well known fact that the acid group is hydrophilic while the hydrocarbon tail is hydrophobic.

When we add isopropanol to the water-oil mixture, the situation changes, as shown in Fig. 3. Water and isopropanol are miscible, and their behaviour is similar as in a pure water-isopropanol solution. Oil molecules are mostly surrounded by isopropanol, which can be easily inferred from the radial distribution functions. On the other hand, the double bonds in the oil clusters tend to be in contact with each other.

Oil in the presence of water and cytochrome P450 behaves similarly as in water-oil solutions, cf. Fig. 4. After a few nanoseconds a clear phase separation takes place, where oil forms an ordered, separate phase. Cytochrome P450 stays solvated in water and in contact with the oil phase only at specific points. At the beginning of the simulation there are several oil molecules in the vicinity of cytochrome P450 at favourable contact sites. These molecules maintain their contact with the enzyme during the whole simulation in a position where an interaction with the active centre (which is situated within the heme group) is possible.

### 3.4 Computational demands

The computational demands of our simulations were highly dependent on the type of simulation. For the energy minimization simulations, it was sufficient to use a single processor for several minutes. For equilibration, we used 16 CPUs running in parallel for a maximum of 3.5 hours. The most demanding simulations during production required 256 CPUs running for 180 hours and a virtual RAM of 2.8 GB.

## 4 Vapour-liquid interfaces and wetting of component surfaces

### 4.1 Planar vapour-liquid interfaces

For simulating vapour-liquid coexistence on the molecular level, a long range correction is needed to obtain accurate results. Thereby, the dispersive contribution to the potential energy  $U_i$  of a molecule  $i$

$$U_i = \sum_{r_{ij} < r_c} u_{ij} + U_i^{LRC} \quad (2)$$

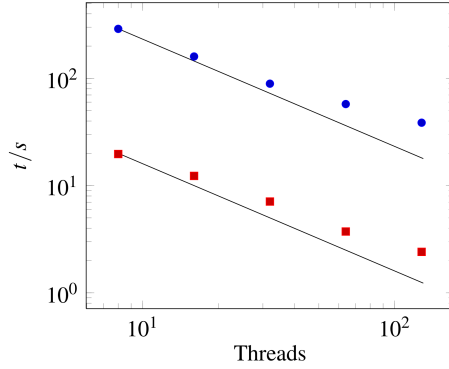


**Fig. 5** Strong scaling with  $N = 256\,000$  2CLJ particles and 512 slabs. The blue dots denote the run time of the whole program, while the red dots only denote the run time of the long range correction. The solid lines represent ideally linear scaling.

is calculated as a sum of the explicitly computed part and the long range correction (LRC), where the latter consists of a summation over  $N_s$  slabs, employing a periodic boundary condition. The LRC is only applied in the direction normal to the planar interface, corresponding to the  $y$  direction here

$$U_i^{LRC} = \sum_k^{N_s} \Delta u_{i,k}^{LRC}(y_i, y_k), \quad (3)$$

given that the system is homogeneous in the other directions. The correction terms  $\Delta u_{i,k}^{LRC}(y_i, y_k)$  for the slabs are calculated as an integral over the slab volume. The resulting term for the potential energy only depends on the distance between the slabs  $r$ , the density  $\rho$  and the thickness  $\Delta y$  of the slabs [29]. The slabwise interaction is computed in pairs, so that  $\frac{1}{2}N_s^2$  individual contributions have to be computed.

Usually, the number of threads is much smaller than the number of slabs. For a scaling test, a system with  $N = 256\,000$  two-centre Lennard-Jones (2CLJ) particles was simulated with different numbers of threads and 512 slabs. Fig. 5 shows the results for the strong scaling behaviour.

For small numbers of threads, the program scales almost ideally, i.e. linearly. For larger numbers of threads, the communication between the threads and the decomposition of the particles becomes more time consuming. Eventually, the long range correction requires even more communication between the threads than the rest of the program, since the density profile has to be sent to every thread before the slab interaction begins. After the slab interaction has been calculated, the correction terms for the potential energy, the force and the virial have to be distributed to every thread.

On the basis of the long range correction discussed above, vapour-liquid equilibria were considered by explicit MD simulation of the fluid phase coexistence (i.e. including an interface), so that the vapour-liquid surface tension  $\gamma$  could be computed following the virial route. For the (single centre) LJ fluid, a high precision

was obtained by simulating  $N = 300\,000$  particles over roughly a million time steps, resulting in very small statistical uncertainties. From the resulting surface tension values, the regression term

$$\gamma = 2.94 \left(1 - \frac{T}{T_c}\right)^{1.23} \frac{\varepsilon}{\sigma^2} \quad (4)$$

was obtained, where the LJ critical temperature is given by Pérez Pellitero *et al.* [30] as  $T_c = 1.3126 \varepsilon$ .

## 4.2 Curved vapour-liquid interfaces

The influence of curvature on vapour-liquid interfacial properties was examined for the truncated-shifted Lennard-Jones fluid (TSLJ), with a cutoff radius of  $r_c = 2.5 \sigma$ , by simulating both curved (i.e. bubble and droplet) as well as planar interfaces by MD simulation of the canonical ensemble at a reduced temperature of  $T = 0.75 \varepsilon$ . For the system with planar symmetry, half of the simulation volume was filled with vapour and the other half with liquid, using a simulation box with a total elongation of  $17 \sigma$ . The density profile from this simulation was compared with that of a bubble with an equimolar radius of  $R_\rho = 12.6 \sigma$  as well as a droplet with  $R_\rho = 12.4 \sigma$ , cf. Fig. 6. A system containing a bubble is subsaturated, whereas the fluid phases coexisting at the curved interface of a droplet are supersaturated with respect to the thermodynamic equilibrium condition for the bulk phases coexisting at saturation. In agreement with this qualitative statement from phenomenological thermodynamics, the vapour density (i.e. the minimal value from the density profile) was found to be smaller for the system containing a bubble ( $\rho'' = 0.0097 \sigma^{-3}$ ) and larger for the system containing a droplet ( $0.0140 \sigma^{-3}$ ), whereas the vapour density over the planar interface was  $0.0127 \sigma^{-3}$ .

Analogous results were obtained for the chemical potential  $\mu^{\text{total}} = \mu^{\text{id}} + \mu^{\text{conf}}$ , which was determined as the sum of the ideal contribution  $\mu^{\text{id}} = T \ln \rho$  and the configurational contribution  $\mu^{\text{conf}}$ . The Widom test particle method [31] was implemented to compute a profile of  $\mu^{\text{conf}}$ , which in equilibrium is complementary to the logarithmic density profile, yielding an approximately constant profile for the total chemical potential, cf. Fig. 6. For the droplet, an average value of  $\mu^{\text{total}} = (-3.31 \pm 0.04) \varepsilon$  was determined, in comparison to  $(-3.51 \pm 0.02) \varepsilon$  for the bubble and  $(-3.37 \pm 0.02) \varepsilon$  for the planar slab. This shows that in the present case, curvature effects are more significant for a gas bubble than for a liquid droplet of the same size, suggesting that the surface tension of the bubble is larger than that of the droplet.

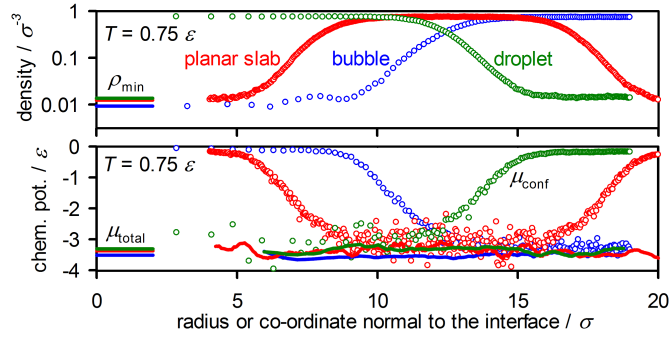


**Fig. 6** Density profiles (top) and chemical potential profiles (bottom) for nanoscopic vapour-liquid interfaces of the TSLJ fluid from canonical ensemble MD simulation of systems containing planar liquid and vapour slabs, a liquid drop (surrounded by a supersaturated vapour), or a gas bubble (surrounded by a subsaturated liquid), respectively. The chemical potential profile includes information on both the configurational contribution (circles) and the total chemical potential (solid lines), as a function of the characteristic spatial coordinate of the system. The solid lines in the bottom left part of the two diagrams indicate the density of the vapour phase (top) as well as the average value of the total chemical potential (bottom).

### 4.3 Temperature dependence of contact angles

The research on the wetting behaviour of surfaces is an active field in materials science. The goal is to reliably predict the wetting properties of component surfaces for design of components with new functional features. In this regard molecular simulations are particularly useful due to their high resolution. Moreover, molecular simulation permits the systematic investigation of the influence of particular parameters on the wetting behaviour.

For the present study, the TSLJ potential was employed and the contact angle dependence on temperature for a non-wetting ( $\theta > 90^\circ$ ) and a partially wetting ( $\theta < 90^\circ$ ) scenario, cf. Fig. 7 was investigated by MD simulation. The solid wall was represented by a face centered cubic lattice with a lattice constant of  $a = 1.55 \sigma$  and the (001) surface exposed to the fluid. For the unlike interaction between the solid and the fluid phase the size and energy parameters  $\sigma_{sf} = \sigma_{ff}$  and

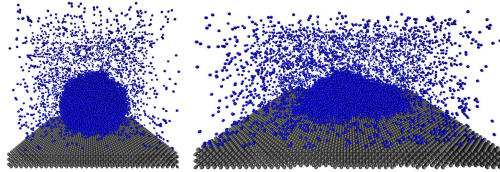


**Fig. 7** Snapshots of simulation runs at different fluid-solid interaction parameters  $\zeta$  of 0.35 (left) and 0.65 (right) at a temperature of  $0.8 \epsilon/k$ .

$$\varepsilon_{\text{sf}} = \zeta \varepsilon_{\text{ff}}, \quad (5)$$

respectively, were applied.

The simulations were carried out with the massively parallel MD program *ls/mardyn* [32]. A total number of  $N = 15\,000$  fluid particles was simulated in the  $NVT$  ensemble. In most cases, 64 processes were employed for parallel computation. The efficient simulation of heterogeneous systems, containing vapour-liquid interfaces and even a solid component, was facilitated here by a dynamic load balancing scheme based on  $k$ -dimensional trees [32]. At the beginning of the simulation, the fluid particles were arranged on regular lattice sites in form of a cuboid. The equilibration time of the three phase system was 2 ns, whereas the total simulation time was chosen to be 6 ns. Periodic boundary conditions were applied in all directions, leaving a channel with a distance of at least  $35\sigma$  between the wall and its periodic image, avoiding “confinement effects” at near-critical temperatures [33]. The contact angles were determined by the evaluation of density profiles averaged over a time span of 4 ns.

Sessile drops were studied at two different interaction parameters,  $\zeta = 0.35$  and  $0.65$ , corresponding to partially wetting and non-wetting conditions. The simulations were carried out in the temperature range between  $0.7$  and  $1\ \varepsilon$ , covering nearly the entire regime of stable vapour-liquid coexistence for the TSLJ fluid, as indicated by the triple point temperature  $T_3 \approx 0.65\ \varepsilon$ , cf. van Meel *et al.* [34], and the critical temperature  $T_c \approx 1.078\ \varepsilon$ , cf. Vrabec *et al.* [35]. It is well known that the respective wetting behaviour of the system, i.e. wetting or dewetting, is reinforced at higher temperatures, cf. Fig. 8. Close to the critical point of the fluid, the phenomenon of critical point wetting occurs [36], i.e. either the liquid or the vapour phase perfectly wets the solid surface

$$|\cos \theta(T \rightarrow T_c)| \rightarrow 1. \quad (6)$$

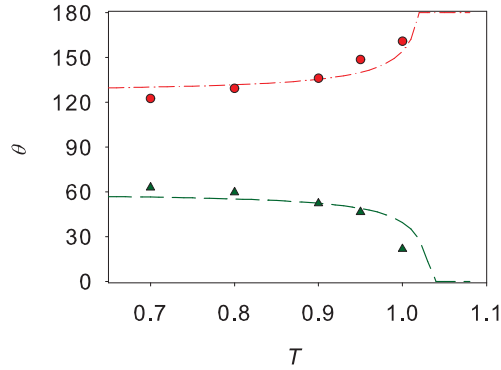


**Fig. 8** Simulation results and correlation for the dependence of the contact angle on the temperature for fluid-solid dispersive interaction strengths  $\zeta$  of  $0.35$  (circles, dashed line) and  $0.65$  (triangles, dash-dotted line).

## 5 Conclusion

Within the MOCOS project, a substantial progress was made regarding software development for massively-parallel molecular simulation. In particular, suitable algorithms for the long range contributions to the intermolecular interaction were implemented in *ms2* (Ewald summation) and *ls1 mardyn* (Janeček correction for long range dispersive effects). In *ls1 mardyn*, a  $k$ -dimensional tree-based domain decomposition with dynamic load balancing was implemented to respond to an uneven distribution of the interaction sites over the simulation volume. Furthermore, *GROMACS* [26] was used to simulate large molecules, taking their internal degrees of freedom into account. In this way, systems with up to 300 000 interaction sites were simulated for over 20 nanoseconds.

New models were developed for alkali cations and halide anions in order to treat the dispersive interaction accurately in molecular simulations of electrolyte solutions. These models were optimized by adjusting the LJ size parameter to the reduced density of aqueous solutions and the energy parameter to diffusion coefficients as well as pair correlation functions. On this basis, quantitatively reliable results were obtained regarding the structure of the hydration shells formed by the water molecules surrounding these ions. Important qualitative structural information on biomolecules at oil-water interfaces was deduced by analysing MD simulations of the cytochrome P450 enzyme, and the critical wetting behaviour as well as the properties of planar and curved vapour-liquid interfaces were characterized by massively-parallel MD simulation with the *ls1 mardyn* program.

The scenarios discussed above show how molecular modelling can today be applied to practically relevant systems even if they exhibit highly complex structures and intermolecular interactions, including significant long range contributions. In the immediate future, molecular simulation as an application of high performance computing will therefore be able to play a crucial role not only by contributing to scientific progress, but also in its day-to-day use as a research and development tool in mechanical and process engineering as well as biotechnology.

**Acknowledgements** The present work was carried out under the auspices of the Boltzmann-Zuse Society for Computational Molecular Engineering (BZS), and the molecular simulations were conducted on the XC4000 supercomputer at the Steinbuch Centre for Computing, Karlsruhe. The authors would like to thank Akshay Bedhotiya (Bombay) for his assistance regarding the simulation of gas bubbles and Sergey Lishchuk (Leicester), Martin Buchholz, Wolfgang Eckhardt, and Ekaterina Elts (München) and Gábor Rutkai (Paderborn) as well as Martin Bernreuther, Colin Glass, and Christoph Niethammer (Stuttgart) for contributing to the development of the *ls1 mardyn* and *ms2* molecular simulation programs as well as Deutsche Forschungsgemeinschaft (DFG) for funding the Collaborative Research Centre (SFB) 926. Furthermore, they would like to acknowledge fruitful discussions with Cemal Engin, Michael Kopnarski, Birgit and Rolf Merz as well as Michael Schappals and Rajat Srivastava (Kaiserslautern), George Jackson and Erich Müller (London), Jonathan Walter (Ludwigshafen), Philippe Ungerer and Marianna Yiannourakou (Paris) as well as Nichola McCann (Visp).

## References

1. S. Deublein, B. Eckl, J. Stoll, S.V. Lishchuk, G. Guevara Carrión, C.W. Glass, T. Merker, M. Bernreuther, H. Hasse, J. Vrabec, *Comput. Phys. Comm.* **182**(11), 2350 (2011)
2. W. Eckhardt, A. Heinecke, R. Bader, M. Brehm, N. Hammer, H. Huber, H.G. Kleinhenz, J. Vrabec, H. Hasse, M. Horsch, M. Bernreuther, C.W. Glass, C. Niethammer, A. Bode, J. Bungartz, in *Proc. ISC 2013* (Springer, Heidelberg, 2013), no. 7905 in LNCS, pp. 1–12
3. M. Horsch, C. Niethammer, J. Vrabec, H. Hasse, *Informat. Technol.* **55**(3), 97 (2013)
4. S. Deublein, S. Reiser, J. Vrabec, H. Hasse, *J. Phys. Chem. B* **116**(18), 5448 (2012)
5. S. Deublein, S. Reiser, J. Vrabec, H. Hasse, submitted (2013)
6. J. Walter, V. Ermatchkov, J. Vrabec, H. Hasse, *Fluid Phase Equilib.* **296**(2), 164 (2010)
7. J. Walter, J. Sehr, J. Vrabec, H. Hasse, *J. Phys. Chem. B* **116**(17), 5251 (2012)
8. Y.L. Huang, T. Merker, M. Heilig, H. Hasse, J. Vrabec, *Ind. Eng. Chem. Res.* **51**(21), 7428 (2012)
9. S. Reiser, N. McCann, M. Horsch, H. Hasse, *J. Supercrit. Fluids* **68**, 94 (2012)
10. S. Pařez, G. Guevara Carrión, H. Hasse, J. Vrabec, *Phys. Chem. Chem. Phys.* **15**(11), 3985 (2013)
11. M. Horsch, H. Hasse, submitted (2013)
12. S. Werth, S.V. Lishchuk, M. Horsch, H. Hasse, *Phys. A* **392**(10), 2359 (2013)
13. S. Werth, G. Rutkai, J. Vrabec, M. Horsch, H. Hasse, in preparation (2013)
14. P.P. Ewald, *Ann. Phys. (Leipzig)* **369**(3), 253 (1921)
15. D. Horinek, S.I. Mamatkulov, R.R. Netz, *J. Chem. Phys.* **130**, 124507 (2009)
16. M.M. Reif, P.H. Hünenberger, *J. Chem. Phys.* **134**, 144104 (2011)
17. M.B. Gee, N.R. Cox, Y.F. Jiao, N. Benteitis, S. Weerasinghe, *J. Chem. Theory Computat.* **7**(5), 1369 (2011)
18. S. Deublein, J. Vrabec, H. Hasse, *J. Chem. Phys.* **136**, 084501 (2012)
19. K. Gubbins, *Statistical Mechanics*, vol. 1 (Burlington House, London, 1972)
20. R. Mills, V. Lobo, *Self-Diffusion in Electrolyte Solutions* (Elsevier, New York, 1989)
21. H. Ohtaki, T. Radnai, *Chem. Rev.* **93**(3), 1157 (1993)
22. J.L. Fulton, D.M. Pfund, S.L. Wallen, M. Newville, E.A. Stern, J. Ma, *J. Chem. Phys.* **105**(6), 2161 (1996)
23. F. Müller Plathe, *ChemPhysChem* **3**(9), 754 (2002)
24. W.L. Jørgensen, D.S. Maxwell, J. Tirado Rives, *J. Am. Chem. Soc.* **110**(45), 11225 (1996)
25. V. Gogonea, J.M. Shy II., P.K. Biswas, *J. Phys. Chem. B* **110**(45), 22861 (2006)
26. S. Pronk, P. Szilárd, R. Schulz, P. Larsson, P. Bjelkmar, R. Apostolov, M.R. Shirts, J.C. Smith, P.M. Kasson, D. van der Spoel, B. Hess, E. Lindahl, *Bioinformatics* **29**(7), 845 (2013)
27. M.E. Tuckerman, G.J. Martyna, *J. Phys. Chem. B* **104**(2), 159 (2000)
28. D. Frenkel, B. Smit, *Understanding Molecular Simulation* (Academic Press, San Diego, 2002)
29. J. Janeček, *J. Phys. Chem. B* **110**(12), 6264 (2006)
30. J. Pérez Pellitero, P. Ungerer, G. Orkoulas, A.D. Mackie, *J. Chem. Phys.* **125**, 054515 (2006)
31. B. Widom, *J. Chem. Phys.* **86**(6), 869 (1982)
32. M. Buchholz, H.J. Bungartz, J. Vrabec, *J. Computational Sci.* **2**(2), 124 (2011)
33. A. Oleinikova, I. Brovchenko, A. Geiger, *Eur. Phys. J. B* **52**(4), 507 (2006)
34. J.A. van Meel, A.J. Page, R.P. Sear, D. Frenkel, *J. Chem. Phys.* **129**, 204505 (2008)
35. J. Vrabec, G.K. Kedia, G. Fuchs, H. Hasse, *Molec. Phys.* **104**(9), 1509 (2006)
36. J.W. Cahn, *J. Chem. Phys.* **66**(8), 3667 (1977)